Score-Based Generative Models Detect Manifolds

Jakiw Pidstrigach
Institut für Mathematik
Universität Potsdam
Karl-Liebknecht-Str. 24/25
14476 Potsdam
pidstrigach@mailbox.org

Abstract

Score-based generative models (SGMs) need to approximate the scores $\nabla \log p_t$ of the intermediate distributions as well as the final distribution p_T of the forward process. The theoretical underpinnings of the effects of these approximations are still lacking. We find precise conditions under which SGMs are able to produce samples from an underlying (low-dimensional) *data manifold* $\mathcal{M}$. This assures us that SGMs are able to generate the "right kind of samples". For example, taking $\mathcal{M}$ to be the subset of images of faces, we find conditions under which the SGM robustly produces an image of a face, even though the relative frequencies of these images might not accurately represent the true data generating distribution. Moreover, this analysis is a first step towards understanding the generalization properties of SGMs: Taking $\mathcal{M}$ to be the set of all training samples, our results provide a precise description of when the SGM memorizes its training data.

1 Introduction

Score-based generative models, also called diffusion models ([Sohl-Dickstein et al., 2015, Song and Ermon, 2019, Song et al., 2021b, Vahdat et al., 2021]) and the related models ([Bordes et al., 2017, Ho et al., 2020, Kingma et al., 2021]) have shown great empirical success in many areas, such as image generation ([Jolicoeur-Martineau et al., 2021, Nichol and Dhariwal, 2021, Dhariwal and Nichol, 2021, Ho et al., 2022]), audio generation ([Chen et al., 2021, Kong et al., 2021, Jeong et al., 2021, Popov et al., 2021]) as well as in other applications ([Batzolis et al., 2021, De Bortoli et al., 2021, Zhou et al., 2021, Cai et al., 2020, Luo and Hu, 2021, Meng et al., 2021, Saharia et al., 2021, Li et al., 2022, Sasaki et al., 2021]). Recently some progress has been made to bridge the gap between the different approaches ([Song et al., 2021b, Huang et al., 2021]) through the framework of SDEs and reverse SDEs.

In generative modelling one is given samples $\{x^i\}_{i=1}^N$ from a measure μ_{data}. The task is to learn a measure μ_{sample} which approximates μ_{data}. The performance of a generative model can then be measured by the distance from μ_{sample} to μ_{data}. In practice however, the true data generating distribution μ_{data} is unknown. All that is known are the samples $\{x_i\}_{i=1}^n$, which can be used to define the empirical measure $\hat{\mu}_{\text{data}}$,

$$\hat{\mu}_{\text{data}} := \text{Unif}\{x^1, x^2, \dots, x^n\}.$$

Any sample from the empirical measure $\hat{\mu}_{\text{data}}$ will be equal to a training example. Hence, while μ_{sample} being close to μ_{data} is the final goal, μ_{sample} being close to $\hat{\mu}_{\text{data}}$ implies that the generative model has memorized the training data. To summarize, a good generative model will output a measure μ_{sample} which is as close to μ_{data} as possible, while keeping some distance from $\hat{\mu}_{\text{data}}$, even though it only knows μ_{data} through $\hat{\mu}_{\text{data}}$.

36th Conference on Neural Information Processing Systems (NeurIPS 2022).

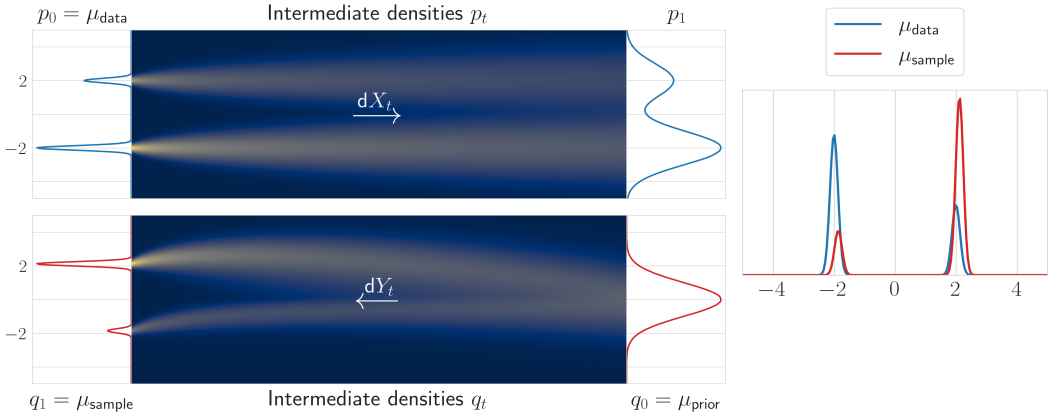

Figure 1: *Top left*: The leftmost plot shows the true data distribution μ_{data} which is a Gaussian mixture. The heat maps show the intermediate densities p_t of X_t, followed by line plots of p_t for $t = 1$.
Bottom left: The rightmost plot shows μ_{prior}, which is a standard Gaussian and differs from p_1. We start the reverse SDE (2) in μ_{prior}. But instead of using the real score, we introduce an approximation error and use $s(x,t) = \nabla \log p_{1-t}(x) + 3$ with a constant error of 3. Again, the heat maps show how the densities q_t of Y_t evolve backwards in time. The leftmost plot shows the resulting distribution q_1 which is used as sample distribution, $\mu_{\text{sample}} = q_1$.
Right: The densities μ_{data} and μ_{sample} are shown for direct comparison. We see that the approximation errors in μ_{prior} and the drift lead to an incorrect sample distribution $\mu_{\text{sample}} \neq \mu_{\text{data}}$. Nevertheless, μ_{sample} is supported in the same area as μ_{data}. For details on the numerical implementation see Appendix B.

Given a target measure π_0, a score-based generative model (SGM) employs two stochastic differential equations (SDEs). The first one is called the *forward SDE*

$$\begin{aligned} \mathrm{d}X_t &= \beta(X_t)\mathrm{d}t + \sigma \mathrm{d}W_t, \\ X_0 &\sim \pi_0. \end{aligned} \tag{1}$$

The marginals of X_t are denoted by π_t. The forward SDE is run until some terminal time T. Furthermore, the *reverse SDE* is defined by

$$\begin{aligned} \mathrm{d}Y_t &= -\beta(Y_t)\mathrm{d}t + \sigma\sigma^T \nabla \log p_{T-t}(Y_t)\mathrm{d}t + \sigma \mathrm{d}B_t, \\ Y_0 &\sim q_0. \end{aligned} \tag{2}$$

We refer to the marginals of Y_t as q_t. The samples are generated from the final distribution q_T, i.e. $\mu_{\text{sample}} := q_T$. The reverse SDE has the property that if q_0 is chosen to be equal to π_T, then $q_t = \pi_{T-t}$. In particular, this implies that $q_T = \pi_0$. Therefore, if we have samples from π_T, we can run the reverse SDE on them to create new samples from π_0.

In the following we will denote by p_t the marginals of the forward SDE when started in the true data generating distribution $\pi_0 = \mu_{\text{data}}$. We will denote by $\hat{p}_t$ the marginals of the forward SDE when started in $\pi_0 = \hat{\mu}_{\text{data}}$. Optimally, we would like to run the algorithm using $\pi_0 = \mu_{\text{data}}$, i.e. with marginals $\pi_t = p_t$. This is however not possible, since μ_{data} itself is unknown.

To circumvent the problem of not knowing p_T, the forward SDE is chosen such that it forgets its initial condition p_0. At time T, the marginal p_T is then well approximated by a proxy distribution $\mu_{\text{prior}} \approx p_T$, independently of p_0. Additionally, the marginals p_t and therefore the scores $\nabla \log p_t$ cannot be evaluated for $p_0 = \mu_{\text{data}}$. Therefore, the scores are replaced by a neural network $s_\theta(x,t)$, which is trained via score-matching techniques [Vincent, 2011, Hyvärinen and Dayan, 2005].

As a result, SGMs make two approximations. The first one is in approximating p_T by μ_{prior}. The second one is the approximation of $\nabla \log p_t$ by the neural net $s_\theta(x,t)$. We illustrate this in Figure 1. It is important to understand how these approximations translate to the distance of μ_{sample} to μ_{data} or $\hat{\mu}_{\text{data}}$.

Some early works already deal with these questions. In [De Bortoli et al., 2021] the total variation distance between μ_{sample} and μ_{data} in bounded, whereas [Song et al., 2021a] derives bounds with

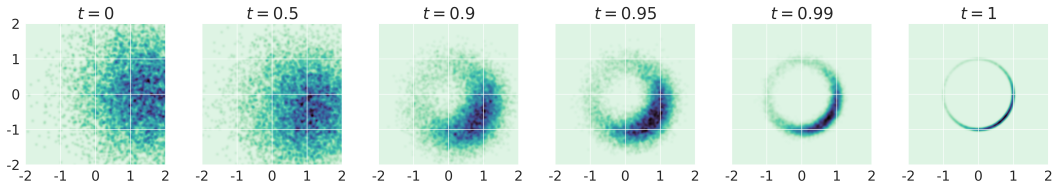

(a) Here μ_{data} is chosen as the uniform distribution on the unit sphere $\mathcal{S}^1$. We use the Brownian motion for the forward SDE. We can compute the exact score $\nabla \log p_t(x)$. We perturb it with the vector $v = (x = 0, y = -1)$ and define the approximation $s(x,t) = \nabla \log p_t(x) + v$. Furthermore, we purposely adopt a poor approximation $\mu_{\text{prior}} \not\approx p_1$ by setting $\mu_{\text{prior}} = \mathcal{N}(m, I)$, where $m = (x = 1.5, y = 0)$. We then run the reverse SDE (8). The figure shows heat maps of the intermediate distributions q_t of the reverse SDE. At time $t = 1$ we reach $q_1 = \mu_{\text{sample}}$. We see that μ_{sample} is a distribution on $\mathcal{M} = \mathcal{S}^1$, albeit not the uniform one. Furthermore, we can observe how the errors in the initial conditions and the drift influence the skewed distribution μ_{sample}. The initial conditions where chosen to have a to large x-coordinate on average, whereas the drift was chosen as to prefer lower y-coordinates. The distribution μ_{sample} is concentrated in areas with high x and low y-coordinates.

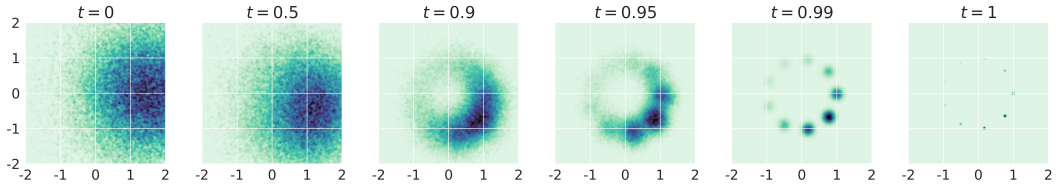

(b) The above experiment is repeated but with μ_{data} chosen to be the uniform distribution on $\mathcal{M} = \{x_i\}_{i=1}^9$, where the x_i are 9 evenly spaced points on the unit sphere $\mathcal{S}^1$. Notice that while the approximation errors cause a non-uniform distribution the training examples, μ_{sample} is still supported solely on $\mathcal{M}$ and will not generate novel samples.

Figure 2: Perturbing $\nabla \log \hat{p}_t$.

respect to the KL-Divergence. The work [De Bortoli et al., 2021] furthermore derives a result similarly to the second part of Theorem 1, but also treating the errors that are introduced by discretizing the SDE. However, both of these works assume that the initial distribution μ_{data} is rather well behaved. In particular, it is assumed that $\mu_{\text{data}}(x) > 0$ for all x. We shortly discuss this assumption now.

Assuming that $\mu_{\text{data}}(x) > 0$ for any x means that one postulates that every x is a possible sample from μ_{data}. For example, this implies that even if all samples $\{x_1, \dots, x_n\}$ of μ_{data} consist of images of human faces, we say that μ_{data} can possibly also generate images of for example furniture, animals or pure white noise. Even though it might have low probability, any combinations of pixels is a possible sample from μ_{data}. The assumption that μ_{data} is actually supported on some lower dimensional substructure $\mathcal{M}$ is well known under the name *manifold hypothesis*, see for example [Bengio et al., 2013, Pope et al., 2021]. In practice this means that $\mu_{\text{data}}(x) = 0$ for many x. This also leads to exploding scores $\nabla \log p_t$ as $t \to 0$ (see Section 5), a behaviour which also observed empirically and further underpins the relevance of the manifold assumption. We will from now on denote the support of μ_{data} as *data manifold* $\mathcal{M}$.

A fundamental question is then: What is the support of μ_{sample} and how does it compare to $\mathcal{M}$. This is interesting for multiple reasons. On the one hand, if we for example assume that $\mathcal{M}$ is the set of all images of faces, then the knowledge that μ_{sample} also has support $\mathcal{M}$ implies that, regardless of how close μ_{sample} actually is to μ_{data}, it will at least always produce an image of a face. On the other hand, we can also compare the support of μ_{sample} to that of $\hat{\mu}_{\text{data}}$. The measures μ_{sample} and μ_{data} sharing their support translates to μ_{sample} memorizing the training data and not being able to generalize. Both of these are very valuable insights into the qualities of μ_{sample} on its own. Furthermore, statistical distances like the KL-Divergence or the total variation distance are only meaningful if the support of the measures overlap to some degree, as otherwise they will equal the maximum distance value.

If two measures have the same support, they are said to be *equivalent*. Our main result is the following:

Main result. *We identify conditions under which μ_{sample} is able to learn the data manifold, that is $supp(\mu_{sample}) = supp(\mu_{data})$. Applying these results to different settings, we find precise conditions*

under which an SGM memorizes its training data or under which it is able to learn the right data manifold $\mathcal{M}$.

In particular we find that for SGMs to be able to generalize, the approximation error made when approximating the training drift $\nabla \log \hat{p}_t$ has to be unbounded.

A first illustration of these results is given in Figure 2. We use a simple example, where we can perfectly evaluate the true drift $\nabla \log \pi_t$. We then choose an incorrect initial condition μ_{prior} which is far from p_T, and also add a constant error to $\nabla \log \pi_t(x)$. The initial measures π_0 are given as the uniform distribution on the unit sphere and the uniform distribution on 9 samples from the unit sphere in Figure 2a and Figure 2 respectively. We see that the final distribution of the reverse SDE, μ_{sample}, is not the uniform distribution anymore. This is due to errors in the initial conditions and the drift. Nevertheless, μ_{sample} is still supported on the exact same subset as π_0.

When applying our main result to the empirical measure $\hat{\mu}_{\text{data}}$ one gets the following corollary, supplying precise conditions under which a SGM has memorized its training data.

Corollary 1. *Denote by $\hat{X}_t$ the forward SDE when started in the empirical measure $\pi_0 = \hat{\mu}_{data}$. Let $\int_0^T \|s_\theta(\hat{X}_t, t) - \nabla \log \hat{p}_t(\hat{X}_t)\mathrm{d}t$ be drift approximation error along a path of the forward SDE. For a given weighting function $w(t)$, the training objective of an SGM can be written as*

$$L_2 = \mathbb{E}_{\hat{X}}[\int_0^T w(t)\|s_\theta(\hat{X}_t, t) - \nabla \log \hat{p}_t(\hat{X}_t)\|^2 \mathrm{d}t], \tag{3}$$

see Section 3. Simultaneously, if the exponential integral of the drift approximation error is integrable in the following sense:

$$L_{\exp} = \mathbb{E}_{\hat{X}}[\exp(\frac{\sigma}{2}\int_0^T \|s_\theta(\hat{X}_t, t) - \nabla \log \hat{p}_t(X_t)\|^2 \mathrm{d}t)] < \infty, \tag{4}$$

the SGM has memorized its training data. Therefore, while training an SGM one should aim to minimize the mean squared error 3 while ensuring that the mean exponential error stays infinite, $L_{\exp} = \infty$.

In particular, if $\|s_\theta(\hat{X}_t, t) - \nabla \log \hat{p}_t(X_t)\|$ is bounded, then $L_{\exp}$ is finite. Therefore, the the generalization capability of a SGM crucially depends on the training error being unbounded.

We now proceed as follows. In Section 2 we will summarize some of the most popular forward SDEs that are applied in SGMs. Then, in Section 3 we discuss how the drift approximation $s_\theta(x, t)$ for SGMs is trained in most implementations. We are ready to state our main results in Section 4. In Section 5 we show how the empirically observed drift explosion is related to the the manifold hypothesis. Most of the paper discusses the error in the drift approximation. But as we have discussed, we also have an error in the initial conditions. In Section 6 we will discuss how large the error in the initial conditions will be in practice.

2 Popular SDEs used in SGMs

In this section we introduce some of the most popular SDEs that are used when implementing SGMs. The first works on SGMs studied discrete forward and backward processes. Nevertheless, the transition kernels and algorithms proposed in those works can be seen as discretisations of some well-known SDEs. More recent works have studied this connection and state the algorithms in terms of SDEs ([Song et al., 2021b, Huang et al., 2021]).

Brownian Motion: The works [Song and Ermon, 2019, 2020] can be seen as a discretization of the SDE

$$\mathrm{d}X_t = \sigma(t)\mathrm{d}W_t.$$

Denoting $h(t) = \int_0^t \sigma(s)\mathrm{d}s$, the solution to the above process can be explicitly stated as a time-changed Brownian motion, $X_t = W_{h(t)}$. The time-change can help in the implementation but does not alter the qualitative behaviour of the reverse SDE. In our following analysis we therefore set $\sigma(t) = 1$. Nevertheless, our results still hold for any positive $\sigma(t)$.

Ornstein-Uhlenbeck Process: The works [Sohl-Dickstein et al., 2015, Ho et al., 2020] can be seen as a discretization of

$$\mathrm{d}X_t = -\frac{1}{2}\alpha(t)X_t\mathrm{d}t + \sqrt{\alpha(t)}\mathrm{d}W_t,$$

which is an Ornstein-Uhlenbeck process. Again, the parameters α_t are a time-change and do not influence the properties that we are investigating in this paper. Therefore, to simplify notation, we again set $\alpha(t) = 1$.

Critically Damped Langevin Dynamics (CLD): The work [Dockhorn et al., 2021] studies a second order SDE. Here artificial velocity coordinates V_t are introduced and the system under consideration is

$$\begin{aligned} \mathrm{d}X_t &= V_t, \\ \mathrm{d}V_t &= -X_t - 2V_t + 2\mathrm{d}W_t, \end{aligned}$$

where $X_0 \sim p_{\text{data}}$, $V_0 \sim \mathcal{N}(0, I)$. For generation one runs the reverse SDE in X_t and V_t but discards the V coordinate at the end. The work [Dockhorn et al., 2021] also includes the parameters M and γ. We set both to 1 as they do in their numerical experiments.

3 Score approximation with a finite number of samples

We now quickly discuss how the neural network is trained to approximate $\nabla \log p_t$ and what implications this has. The score $\nabla \log p_t$ is approximated by minimizing a variant of

$$L(\theta) = \int_0^T w(t)\, \mathbb{E}_{p_t(x)}[\|\nabla \log p_t(x) - s_\theta(x,t)\|^2]\mathrm{d}t. \tag{5}$$

for some weighting function w. The optimization is done via score matching techniques (see [Hyvärinen and Dayan, 2005, Vincent, 2011, Song et al., 2020]). However, the above expectation depends on p_t, which we cannot evaluate since it depends on $p_0 = \mu_{\text{data}}$. Nevertheless, we can evaluate the approximation $\hat{p}_t$,

$$\hat{p}_t(x) = \mathbb{E}_{\hat{\mu}_{\text{data}}(x_0)}[p_{t|0}(x|x_0)] = \frac{1}{N}\sum_{i=1}^{N} p_{t|0}(x|x^i) \approx p_t(x) = \mathbb{E}_{\mu_{\text{data}}}[p_{t|0}(x|x_0)]. \tag{6}$$

The surrogate loss

$$\hat{L}(\theta) = \int_0^T w(t)\, \mathbb{E}_{\hat{p}_t(x)}[\|\nabla \log \hat{p}_t(x) - s_\theta(x,t)\|^2]\mathrm{d}t, \tag{7}$$

can be evaluated and is used for training. The equation (7) is equivalent to (3) since $\hat{X}_t$ has distribution $\hat{p}_t$. If we would minimize this loss perfectly, then $s_\theta(x,t)$ would be equal to $\nabla \log \hat{p}_t$. The reverse SDE started in an appropriate initial condition with drift $\nabla \log \hat{p}_t$ however, will produce samples from $\hat{\mu}_{\text{data}}$, which are training examples. This raises the question in which way or to which degree the loss should actually be minimized.

4 Effects of the approximations

This section contains our main results. We first state the assumptions we have to make and then the Theorems.

4.1 Error in the initial condition

The following assumption is needed for the reverse SDE to be defined even in the case when the initial distribution π_0 has a degenerate support. In Lemma 1 we will show that all the SDEs from Section 2 satisfy the Assumption.

Assumption 1. *There is a constant C such that*

(i) β is globally Lipschitz, i.e. $\|\beta(x) - \beta(y)\| \leq C\|x - y\|$.

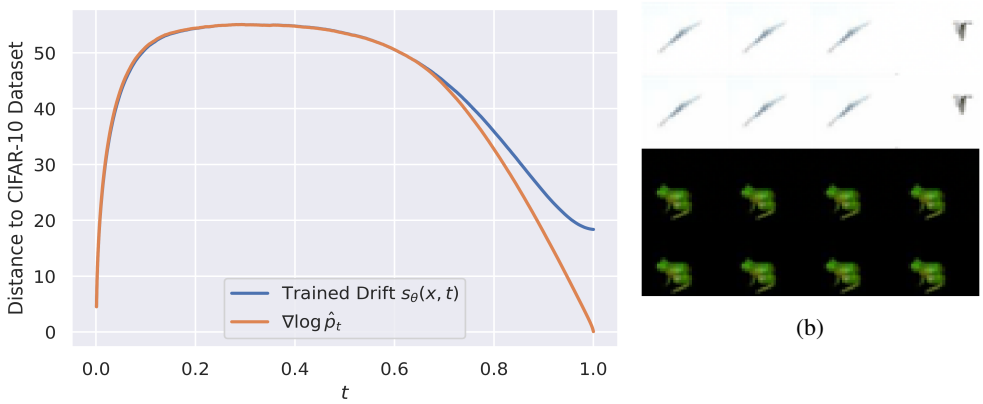

(a) (b)

Figure 3: (a): Both lines correspond to the same experiment for different drifts in the reverse SDE. For both lines we started $N = 1000$ paths in the zero vector in $\mathbb{R}^{32\times32\times3}$. For the blue line we used the pretrained CIFAR-10 DDPM++ model from Song et al. [2021b], whereas for the orange line we used the true drift $\nabla \log \hat{p}_t$, which is a mixture of 50000 Gaussians, one for each training example in CIFAR-10. We then saved the distance from Y_t to the CIFAR-10 training examples, by calculating the distance to the closest example. Above we plot the average distance. We see, that while the reverse SDE run with $\hat{p}_t$ will have a distance of 0 to the training examples in the end, the SDE with the pretrained drift keeps some distance to the training examples and therefore produces novel images. (b): We evaluate $\nabla \log \hat{p}_t$ as in (a). We do the analogous experiment to Figure 2b on CIFAR-10 and perturb the empirical drift $\nabla \log \hat{p}_t$ with a constant error vector. The first row shows the samples generated by adding the constant error vector $e(x,t) = (1, 1, \dots, 1) \in \mathbb{R}^{32\times32\times3}$ to $\nabla \log \hat{p}_t$. In the second row we searched for the closest image in the CIFAR-10 dataset (with respect to the Euclidean 2-distance on $\mathbb{R}^{32\times32\times3}$) and plotted it. We see that all the sampled images are nearly equal to a corresponding image in CIFAR-10. The distance of the images to their closest image in CIFAR-10 is around 0.07 for all plotted images. Similar to Figure 2, we can observe the effect of adding the one-vector. The sample distribution μ_{sample} got skewed to prefer images that have high pixel values. This corresponds to samples which are mostly white for the human eye. In the third and forth row we repeat the experiment of the first and second row, but add the negative one-vector $e(x,t) = (-1, -1, \dots, -1)$ and get black images.

(ii) β *grows at most linearly, i.e.* $\|\beta(x)\| \leq C(1 + \|x\|)$.

(iii) X_t *has a density* $\pi_t \in C^1$ *for every* $t > 0$ *and* $\int_{t_0}^1 \int_{\|x\|<R} |\pi_t(x)|^2 + \|\nabla_x \pi_t(x)\|^2 \mathrm{d}x\mathrm{d}t < \infty$ *for any* $R > 0$ *and* $0 < t_0 \leq T$.

Furthermore, for each $S \in (0, T)$ *and all* x, y *for which* $\|x\|, \|y\| \leq N$ *there is a constant* $C_{S,N}$ *such that*

(iv) $\nabla \log \pi_t$ *is locally Lipschitz,* $\|\nabla \log \pi_t(x) - \nabla \log \pi_t(y)\| \leq C_{S,N}\|x - y\|$ *for all* $t \in [S, T]$.

Conditions (i)-(iii) are technical conditions on the forward SDE. They ensure that if we run a solution to the forward SDE, X_t, backwards in time, then $X_t^R := X_{T-t}$ will be a solution to the reverse SDE (2) on $[0, T)$. The last condition then ensures that the solutions to the reverse SDE are unique, therefore we will be able to transmit the properties of X^R to any other solution Y_t of (2). The following result shows that Assumption 1 can be expected to hold in practice. To simplify the calculations we assume that the data manifold $\mathcal{M} = \text{supp}(\mu_{\text{data}})$ is contained in a ball of diameter M. This is a natural assumption for many data sets. Nevertheless, we note that this assumption could be weakened by additional technical effort.

Lemma 1. *Assume that the data manifold* $\mathcal{M}$ *is contained in a ball of radius* M. *Then all the methods introduced in Section 2 fulfil Assumption 1.*

We are now ready to state our first main result,

Theorem 1. *Denote by π_t the marginals of the forward SDE started in π_0. Assume that Assumption 1 holds and that μ_{prior} is absolutely continuous with respect to π_T. Then the following hold.*

(i) Let Y_t be a solution to (2) on $[0, T)$. The limit $Y_T := \lim_{t\to T} Y_T$ exists almost surely. We refer to its distribution as μ_{sample}. The distribution μ_{sample} is absolutely continuous with respect to μ_{data}. If π_T and μ_{prior} are equivalent, then so are μ_{sample} and π_0.

(ii) Furthermore, for any f-divergence D_f,

$$D_f(\mu_{sample}|\pi_0) \leq D_f(\mu_{prior}|\pi_T) \quad \text{and} \quad D_f(\pi_0|\mu_{sample}) \leq D_f(\pi_T|\mu_{prior}).$$

Applying the above theorem with $\pi_T = p_T$ tells us something about the equivalence and distance between μ_{sample} and μ_{data}, since $\pi_0 = p_0 = \mu_{\text{data}}$. Applying the theorem with $\hat{p}_t$ tells us something about the generalization capabilities of SGMs.

The measures π_T and μ_{prior} are normally both supported on all of $\mathbb{R}^d$ and therefore equivalent. Since Assumption 1 also holds in most situations (see Lemma 1), the requirements for Theorem 1 are satisfied in practice. From item (i) with $\pi_t = \hat{p}_t$ we can conclude that the error we make in the initial conditions is not responsible for the generalization capacities of SGMs.

The second item then shows that the f-divergences between μ_{sample} and μ_{data} are bounded by the f-divergences of μ_{prior} to p_T. The total variation distance and the KL-Divergence are both special cases of f-divergences.

4.2 Error in the drift

Given a forward SDE with marginals π_t and an approximation $s(x, t)$ to $\nabla \log \pi_t$, we define the reverse SDE for the approximation s as

$$\begin{aligned} \mathrm{d}\tilde{Y}_t &= -\beta(\tilde{Y}_t)\mathrm{d}t + \sigma\sigma^T s(\tilde{Y}_t, t)\mathrm{d}t + \sigma \mathrm{d}B_t, \\ \tilde{Y}_0 &\sim q_0. \end{aligned} \tag{8}$$

Assumption 2. *We assume that the reverse SDE $\tilde{Y}_t$ has a solution on $[0, T)$. For $t < T$, we define the Girsanov weights*

$$Z_t = \exp\left(\int_0^t \sigma^T(s(\tilde{Y}_t, t) - \nabla \log \pi_t(\tilde{Y}_t)) \cdot \mathrm{d}B_s - \frac{1}{2}\int_0^t \|\sigma^T(s(\tilde{Y}_t, t) - \nabla \log \pi_t(\tilde{Y}_t))\|^2 \mathrm{d}s\right) \tag{9}$$

and assume that the Z_t are a uniformly integrable martingale.

We shortly discuss this assumption. The assumption that Z_t is a martingale is equivalent to the expectation of Z_t being equal to 1 for all t. The assumption that it is uniformly integrable is more technical (see Appendix A.2), but is fulfilled for example if for some $p > 1$, $\mathbb{E}[|Z_t|^p] < \infty$ for all t. For example, if the Z_t have bounded variance, then they are uniformly integrable.

A condition that ensures that Z_t is both, a martingale and uniformly integrable, is given by *Novikov's condition* Novikov [1980]. It states, that if

$$N_T = \mathbb{E}_{\tilde{Y}}\left[\exp\left(\frac{1}{2}\int_0^T \|\sigma^T(s(\tilde{Y}_t, t) - \nabla \log \pi_t(\tilde{Y}_t))\|^2 \mathrm{d}s\right)\right] < \infty, \tag{10}$$

then Z_t is a uniformly integrable martingale.

Using Assumption 2 we can now state

Theorem 2. *Assume that Assumption 2 holds. Assume furthermore that Assumption 1 holds with $\nabla \log \pi_t$ replaced by $s(x, t)$.*

Then $\tilde{Y}_T = \lim_{t\to T} \tilde{Y}_t$ is well defined. Moreover, its distribution is equivalent to the distribution of Y_T. In particular, if $\|s(x, t) - \nabla \log \hat{p}_t\|$ is bounded, then Assumption 2 holds, and the SGM has memorized its training data.

Putting Theorem 1 and Theorem 2 together, we can conclude that, if both Assumptions hold, μ_{sample} is equivalent to π_0. Therefore, if Assumption 2 holds for $\pi_t = p_t$, we have a positive statement and know that μ_{sample} will have the exact same support as μ_{data}, i.e. it has learned the data manifold $\mathcal{M}$.

If the Assumption would hold for $\pi_t = \hat{p}_t$, we would however just memorize the training data, see Figure 2b or Figure 3b for a visualization. However, empirically it has been shown that SGMs are able to create novel samples (see, Figure 3a or Dhariwal and Nichol [2021]). Therefore, we can deduce that Assumption 2 is violated in practice.

We evaluated N from (10) on CIFAR-10, once for the difference between the $s_\theta(x,t)$ from Song et al. [2021b] and $\nabla \log \hat{p}_t$, and once by just using a perturbed drift with a constant error, $s(x,t) = \nabla \log \hat{p}_t + \frac{1}{2}(1,1,\dots,1)$, see Figure 4. The reverse SDE using the drift $\nabla \log \hat{p}_t + \frac{1}{2}(1,1,\dots,1)$, is equivalent to $\hat{\mu}_{\text{data}}$, as we know from Theorem 2 and have also already observed in Figure 3b. Figure 4 confirms that Z_t is indeed a uniformly integrable martingale and therefore fulfils Assumption 2.

Corollary 1 can be deduced by exchanging the roles of $\tilde{Y}_t$ and Y_t. We then get an equivalent condition to Assumption 2, which is

$$\tilde{N}_T = \mathbb{E}_Y \left[\exp\left(\frac{1}{2} \int_0^T \|\sigma^T (s(Y_t,t) - \nabla \log \pi_t(Y_t))\|^2 \mathrm{d}s \right) \right] < \infty,$$

where the expectation is now taken over the reverse SDE with the correct drift $\nabla \log \pi_t$ instead of the approximate drift s_θ. However, Y is just the time reversal of X, therefore we can also write the above expectation over X_t instead of Y_t. If we treat the case where we start X_t in the empirical measure $\hat{\mu}_{\text{data}}$, π_t will be equal to $\pi_t = \hat{p}_t$ by definition and

$$\mathbb{E}_{\hat{X}} \left[\exp\left(\frac{\sigma^2}{2} \int_0^T \|\sigma^T (s(\hat{X}_t,t) - \nabla \log \hat{p}_t(\hat{X}_t))\|^2 \mathrm{d}s \right) \right] < \infty$$

is a sufficient condition for $\hat{\mu}_{\text{data}}$ and μ_{sample} having the same support. We have here assumed that Theorem 1 can be applied. However, this can be assumed in practice, see the discussion after Theorem 1.

In future work we believe that further understanding the characteristics of Z_t, how they relate to the minimization of $L(\theta)$ and generalization is crucial to the understanding of SGMs and their empirical success. Recent works also study the question on how the neural network architecture and parametrization is related to the boundedness of the output Kim et al. [2022]. The relationship between these choices and the properties of Z_t is also an interesting research avenue. Lastly, the distribution of Z_t is very heavy-tailed. Most of the samples are very small with a few extremely large samples in between. Therefore one needs many samples from Z_t to understand its characteristics. Finding robust estimators for Z_t or its expectation could help their usage in the training or evaluation procedure.

5 Drift Explosion under manifold hypothesis

In practice it is often observed that the drift of the reverse SDE explodes as $t \to T$. see for example Kim et al. [2022, Section 3.1]. We now show how this observed behaviour is related to the manifold hypothesis.

First, we note that all SDEs in Section 2 are linear SDEs. Therefore, their transition kernels are Gaussian ([Pavliotis, 2014, Section 3.7]):

$$\pi_t(X_t = x | X_0 = x_0) = \mathcal{N}(x; m_t(x_0), \Sigma_t).$$

The explicit form of m_t and Σ_t differ for each of the SDEs and can be found in Appendix C.1. We remark that Σ_t does not depend on the initial condition x_0. The transition kernel above is the distribution of the SDE started in a single point x_0. Since we start the SDE in μ_{data} we need to average over μ_{data} to get the marginal at time t:

$$p_t(x) = \int_{\mathbb{R}^d} \mathcal{N}(x; m_t(x_0), \Sigma_t) \mu_{\text{data}}(x_0) \mathrm{d}x_0. \tag{11}$$

We can also compute the additional drift in the reverse SDE (see Appendix C.2),

$$\nabla \log p_t(x) = \frac{\nabla p_t(x)}{p_t(x)} = \Sigma_t^{-1}(x - \mathbb{E}[m_t(X_0)|X_t = x]). \tag{12}$$

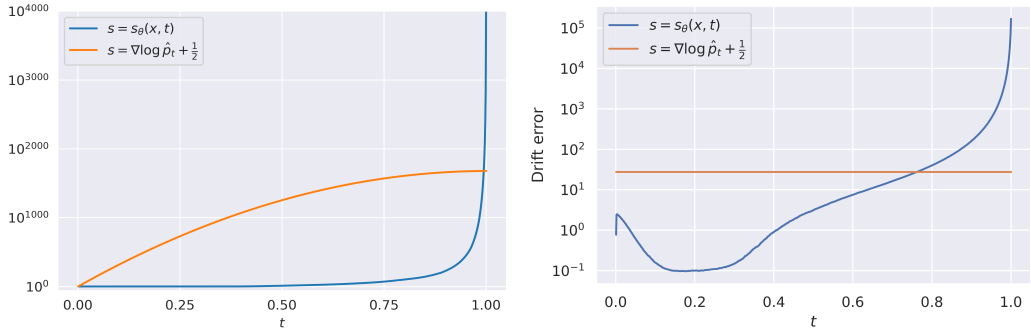

Figure 4: Left: We simulated the reverse SDE on CIFAR-10, once with the pretrained CIFAR-10 DDPM++ model s_θ from Song et al. [2021b] and once with a perturbed drift $s(x,t) = \nabla \log \hat{p}_t + \frac{1}{2}(1, 1, \ldots, 1)$. We then evaluated the integral (10) numerically for varying $t = T$. For the perturbed drift, the integral does not seem to explode as $t \to 1$, implying that Z_t is a martingale. We see that for the DDPM++ drift, the integral explodes, therefore we can not infer that Z_t is a martingale. We used $N = 12000$ simulations from both of the SDEs to generate this plot. Right: We again ran the two SDEs with the drifts as in the left Figure. This time, we measured the average distance to the empirical drift $\|s(\hat{Y}_t, t) - \nabla \log \hat{p}_t(\hat{Y}_t)\|$ along a path of the reverse SDE. We repeated the experiment $N = 2560$ times and plotted the mean distance. For the constant perturbation we also of course get a constant distance. The distance of the true drift to $\nabla \log \hat{p}_t$ is initially very small but explodes as $t \to 1$. From our results we know that this explosion is necessary for the SGM to generalize.

We now want to evaluate $\nabla \log p_t$ along a typical path of Y_t, i.e. we are interested in $\mathbb{E}[\nabla \log p_t(Y_t)]$. The distribution of Y_t however depends on the drift approximation s_θ we use. For this calculation we will assume that we are able to run the reverse SDE with the true drift $s_\theta(x,t) = p_t(x)$. Then however, since Y_t is then just X_t run backwards, they have the same distributions and we can calculate

$$\mathbb{E}[\|\nabla \log p_t(Y_t)\|] = \mathbb{E}[\|\nabla \log p_t(X_t)\|] = \Sigma_t^{-1}\mathbb{E}[\|X_t - \mathbb{E}[m_t(X_0)|X_t = y]\|].$$

If the manifold $\mathcal{M}$ is not to badly behaved, we can expect that for small t and almost all x, $\mathbb{E}[X_0|X_t = x]$ to be very close to the data manifold $\mathcal{M}$. Especially, $\|X_t - \mathbb{E}[X_0|X_t = x]\|$ will be larger than $\text{dist}(X_t, \mathcal{M})$ in that case. However, the distribution of X_t can be represented as $m_t(X_0) + \sqrt{\Sigma_t}\xi$, where ξ has a standard normal distribution. For the SDEs we treated in Section 2, $m_t(X_t)$ is either equal or very close to $m_t(X_t) = X_t$ for small values of t. Finally, if we assume that $\mathcal{M}$ is a subset of relatively low dimension in a high dimensional space, we can expect that with very high probability $\sqrt{\Sigma_t}\xi$ points away from the data manifold. Therefore the distance of X_t to $\mathcal{M}$ can be approximated by $\sqrt{\Sigma_t}\xi$. Putting these approximations together we can calculate

$$\mathbb{E}[\|X_t - \mathbb{E}[m_t(X_0)|X_t = y]\|] \gtrsim \mathbb{E}[\text{dist}(X_t, \mathcal{M})] \gtrsim \|\Sigma_t\|^{1/2}\mathbb{E}[\|\xi\|] \approx \|\Sigma_t\|^{1/2}\sqrt{d},$$

where d is the dimension of the data space in which the samples x_i lie. Therefore we can conclude that

$$\|\nabla \log p_t(Y_t)\| \gtrsim \frac{d^{1/2}}{\|\Sigma_t\|^{1/2}}.$$

For the Brownian motion for example, $\Sigma_t = t$ and therefore the right hand side scales like $\frac{1}{\sqrt{t}}$. If Σ_t is the covariance of p_t, then we can expect $\nabla \log p_t(Y_t)$ to be of order $\frac{1}{\|\Sigma_t\|^{1/2}}$. Furthermore, $\nabla \log p_t(Y_t)$ will point towards the data manifold for small t. The drift $\nabla \log p_t(Y_t)$ then acts like a *support matching force*, where the force grows to infinity as $t \to 0$, absorbing all the SDE paths onto the manifold.

6 Distance from p_T to μ_{prior}

We have seen in Theorem 1 that the distance between μ_{sample} and μ_{data} is directly related to the distance between p_T and μ_{prior} if we neglect the errors made in the approximation of the drift. For both, the OU-Process and the CLD, there are plenty of results on the distance of p_t to $\mathcal{N}(0, I_d)$. In general, one can expect this distance to grown exponentially in time t.

The Brownian motion however does not converge to a stationary distribution and therefore one has to choose a different μ^T_{prior} for each T to approximate p_T. In practice, one normally chooses a normal distribution $p_T = \mathcal{N}(m_t, C_t)$ (see [Song et al., 2021b, Appendix C]). The following Lemma is derives the optimal values for m_t and C_t.

Lemma 2. *Let p_T be the T-time marginal of the Brownian motion process X_t of Section 2. The following minimization problem*

$$\min_{m,C} KL(p_T \mid \mathcal{N}(m, C))$$

is minimized by $m_T = \mathbb{E}[\mu_{data}]$ and $C_T = \mathrm{Cov}[\mu_{data}] + TI_d$. If we restrict the covariance to be a multiple of the identity matrix, the problem is solved by choosing m as above and c as $c = \mathbb{E}[\|X_t - m\|^2] = trace(C_T)$.

This result is a slight variation on the well known fact that the KL-projection in the second argument matches its moments. We prove it in Appendix E.2. The following result shows that the distance between p_T and μ^T_{prior} decreases with time and also gives a rate. It justifies using the Brownian motion and a normal prior distribution for SGMs.

Lemma 3. *Let p_t be the time t-marginal of a Brownian motion with initial condition μ_{data}. Denote by $c_i, i = 1, \dots, d$, the eigenvalues of $\mathrm{Cov}(\mu_{data})$. Let μ^T_{prior} be the normal distribution with mean $m_T = \mathbb{E}[\mu_{data}]$ and covariance $C_T = \mathrm{Cov}[\mu_{data}] + TI_d$. Then*

$$KL(p_T|\mu^T_{prior}) \leq \frac{1}{2} \log \left(\frac{\prod_{i=1}^d (c_i + T)}{T^d} \right).$$

The proof can be found in Appendix E.2.

7 Broader impact

The results deepen the understanding of score-based generative models. As such, they can be seen as a step towards improving the quality of generative models. Therefore the possible negative societal impacts are the same ones that apply to generative modelling in general. First, generative models can be used to create synthetic data that is hard to distinguish from real data (for example images or videos), see [Mirsky and Lee, 2021]. Second, generative models can learn and reproduce biases that are prevalent in the training data ([Esser et al., 2020]). Last, depending on the application, generative models might be used to do creative work that was previously done by humans.

8 Conclusion

We conducted a theoretical study of some properties of SGMs. We found explicit conditions under which the sample measure μ_{sample} is equivalent to the true data generating distribution μ_{data}. Under these conditions we can guarantee, that the SGM generates samples that could also be samples from μ_{data}. Furthermore, each sample that can be generated by μ_{data} also has positive probability under μ_{sample}, meaning that the full support is covered.

Since one can not actually access the full support of μ_{data}, but only a finite number of training examples $\{x_i\}_{i=1}^N$, our results can be applied to find conditions under which the SGM memorizes its training data. We believe that this observation provides a first step towards understanding the generalization capabilities of SGMs.

9 Funding

The author has been partially supported by Deutsche Forschungsgemeinschaft (DFG) - Project-ID 318763901 - SFB1294.

References

G. Batzolis, J. Stanczuk, C. Schönlieb, and C. Etmann. Conditional image generation with score-based diffusion models. *CoRR*, abs/2111.13606, 2021. URL `https://arxiv.org/abs/2111.13606`.

Y. Bengio, A. Courville, and P. Vincent. Representation learning: A review and new perspectives. *IEEE transactions on pattern analysis and machine intelligence*, 35(8):1798–1828, 2013.

F. Bordes, S. Honari, and P. Vincent. Learning to generate samples from noise through infusion training. *arXiv preprint arXiv:1703.06975*, 2017.

R. Cai, G. Yang, H. Averbuch-Elor, Z. Hao, S. J. Belongie, N. Snavely, and B. Hariharan. Learning gradient fields for shape generation. In A. Vedaldi, H. Bischof, T. Brox, and J. Frahm, editors, *Computer Vision - ECCV 2020 - 16th European Conference, Glasgow, UK, August 23-28, 2020, Proceedings, Part III*, volume 12348 of *Lecture Notes in Computer Science*, pages 364–381. Springer, 2020. doi: 10.1007/978-3-030-58580-8_22. URL https://doi.org/10.1007/978-3-030-58580-8_22.

N. Chen, Y. Zhang, H. Zen, R. J. Weiss, M. Norouzi, and W. Chan. Wavegrad: Estimating gradients for waveform generation. In *9th International Conference on Learning Representations, ICLR 2021, Virtual Event, Austria, May 3-7, 2021*. OpenReview.net, 2021. URL https://openreview.net/forum?id=NsMLjcFaO8O.

M. Costa and T. Cover. On the similarity of the entropy power inequality and the Brunn-Minkowski inequality (corresp.). *IEEE Transactions on Information Theory*, 30(6):837–839, 1984.

V. De Bortoli, J. Thornton, J. Heng, and A. Doucet. Diffusion schrödinger bridge with applications to score-based generative modeling. *Advances in Neural Information Processing Systems*, 34, 2021.

P. Dhariwal and A. Nichol. Diffusion models beat gans on image synthesis. *Advances in Neural Information Processing Systems*, 34, 2021.

T. Dockhorn, A. Vahdat, and K. Kreis. Score-based generative modeling with critically-damped Langevin diffusion. *CoRR*, abs/2112.07068, 2021. URL https://arxiv.org/abs/2112.07068.

P. Esser, R. Rombach, and B. Ommer. A note on data biases in generative models. In *NeurIPS 2020 Workshop on Machine Learning for Creativity and Design*, 2020. URL https://arxiv.org/abs/2012.02516.

U. G. Haussmann and E. Pardoux. Time reversal of diffusions. *The Annals of Probability*, pages 1188–1205, 1986.

J. Ho, A. Jain, and P. Abbeel. Denoising diffusion probabilistic models. *Advances in Neural Information Processing Systems*, 33:6840–6851, 2020.

J. Ho, C. Saharia, W. Chan, D. J. Fleet, M. Norouzi, and T. Salimans. Cascaded diffusion models for high fidelity image generation. *Journal of Machine Learning Research*, 23(47):1–33, 2022.

C.-W. Huang, J. H. Lim, and A. C. Courville. A variational perspective on diffusion-based generative models and score matching. *Advances in Neural Information Processing Systems*, 34, 2021.

A. Hyvärinen and P. Dayan. Estimation of non-normalized statistical models by score matching. *Journal of Machine Learning Research*, 6(4), 2005.

M. Jeong, H. Kim, S. J. Cheon, B. J. Choi, and N. S. Kim. Diff-tts: A denoising diffusion model for text-to-speech. In H. Hermansky, H. Cernocký, L. Burget, L. Lamel, O. Scharenborg, and P. Motlícek, editors, *Interspeech 2021, 22nd Annual Conference of the International Speech Communication Association, Brno, Czechia, 30 August - 3 September 2021*, pages 3605–3609. ISCA, 2021. doi: 10.21437/Interspeech.2021-469. URL https://doi.org/10.21437/Interspeech.2021-469.

A. Jolicoeur-Martineau, R. Piché-Taillefer, I. Mitliagkas, and R. T. des Combes. Adversarial score matching and improved sampling for image generation. In *9th International Conference on Learning Representations, ICLR 2021, Virtual Event, Austria, May 3-7, 2021*. OpenReview.net, 2021. URL https://openreview.net/forum?id=eLfqMl3z3lq.

I. Karatzas and S. Shreve. *Brownian motion and stochastic calculus*, volume 113. Springer Science & Business Media, 2012.

D. Kim, S. Shin, K. Song, W. Kang, and I. Moon. Soft truncation: A universal training technique of score-based diffusion model for high precision score estimation. In K. Chaudhuri, S. Jegelka, L. Song, C. Szepesvári, G. Niu, and S. Sabato, editors, *International Conference on Machine Learning, ICML 2022, 17-23 July 2022, Baltimore, Maryland, USA*, volume 162 of *Proceedings of Machine Learning Research*, pages 11201–11228. PMLR, 2022. URL https://proceedings.mlr.press/v162/kim22i.html.

D. P. Kingma, T. Salimans, B. Poole, and J. Ho. Variational diffusion models. *arXiv preprint arXiv:2107.00630*, 2021.

A. Klenke. *Probability theory: a comprehensive course*. Springer Science & Business Media, 2013.

Z. Kong, W. Ping, J. Huang, K. Zhao, and B. Catanzaro. Diffwave: A versatile diffusion model for audio synthesis. In *9th International Conference on Learning Representations, ICLR 2021, Virtual Event, Austria, May 3-7, 2021*. OpenReview.net, 2021. URL https://openreview.net/forum?id=a-xFK8Ymz5J.

A. Krizhevsky, G. Hinton, et al. Learning multiple layers of features from tiny images. 2009.

C. Léonard. Stochastic derivatives and generalized h-transforms of Markov processes. *arXiv preprint arXiv:1102.3172*, 2011.

H. Li, Y. Yang, M. Chang, S. Chen, H. Feng, Z. Xu, Q. Li, and Y. Chen. Srdiff: Single image super-resolution with diffusion probabilistic models. *Neurocomputing*, 479:47–59, 2022. doi: 10.1016/j.neucom.2022.01.029. URL https://doi.org/10.1016/j.neucom.2022.01.029.

F. Liese and I. Vajda. On divergences and informations in statistics and information theory. *IEEE Transactions on Information Theory*, 52(10):4394–4412, 2006.

S. Luo and W. Hu. Diffusion probabilistic models for 3d point cloud generation. In *IEEE Conference on Computer Vision and Pattern Recognition, CVPR 2021, virtual, June 19-25, 2021*, pages 2837–2845. Computer Vision Foundation / IEEE, 2021. URL https://openaccess.thecvf.com/content/CVPR2021/html/Luo_Diffusion_Probabilistic_Models_for_3D_Point_Cloud_Generation_CVPR_2021_paper.html.

C. Meng, Y. Song, J. Song, J. Wu, J. Zhu, and S. Ermon. Sdedit: Image synthesis and editing with stochastic differential equations. *CoRR*, abs/2108.01073, 2021. URL https://arxiv.org/abs/2108.01073.

Y. Mirsky and W. Lee. The creation and detection of deepfakes: A survey. *ACM Computing Surveys (CSUR)*, 54(1):1–41, 2021.

A. Q. Nichol and P. Dhariwal. Improved denoising diffusion probabilistic models. In *International Conference on Machine Learning*, pages 8162–8171. PMLR, 2021.

A. A. Novikov. On conditions for uniform integrability of continuous non-negative martingales. *Theory of Probability & Its Applications*, 24(4):820–824, 1980.

G. A. Pavliotis. *Stochastic processes and applications: diffusion processes, the Fokker-Planck and Langevin equations*, volume 60. Springer, 2014.

S. Peluchetti. Non-denoising forward-time diffusions. 2021.

P. Pope, C. Zhu, A. Abdelkader, M. Goldblum, and T. Goldstein. The intrinsic dimension of images and its impact on learning. In *9th International Conference on Learning Representations, ICLR 2021, Virtual Event, Austria, May 3-7, 2021*. OpenReview.net, 2021. URL https://openreview.net/forum?id=XJk19XzGq2J.

V. Popov, I. Vovk, V. Gogoryan, T. Sadekova, and M. A. Kudinov. Grad-tts: A diffusion probabilistic model for text-to-speech. In M. Meila and T. Zhang, editors, *Proceedings of the 38th International Conference on Machine Learning, ICML 2021, 18-24 July 2021, Virtual Event*, volume 139 of *Proceedings of Machine Learning Research*, pages 8599–8608. PMLR, 2021. URL http://proceedings.mlr.press/v139/popov21a.html.

O. Rioul. Information theoretic proofs of entropy power inequalities. *IEEE Transactions on Information Theory*, 57(1):33–55, 2010.

C. Saharia, J. Ho, W. Chan, T. Salimans, D. J. Fleet, and M. Norouzi. Image super-resolution via iterative refinement. *CoRR*, abs/2104.07636, 2021. URL `https://arxiv.org/abs/2104.07636`.

H. Sasaki, C. G. Willcocks, and T. P. Breckon. UNIT-DDPM: UNpaired image translation with denoising diffusion probabilistic models. *CoRR*, abs/2104.05358, 2021. URL `https://arxiv.org/abs/2104.05358`.

J. Sohl-Dickstein, E. Weiss, N. Maheswaranathan, and S. Ganguli. Deep unsupervised learning using nonequilibrium thermodynamics. In *International Conference on Machine Learning*, pages 2256–2265. PMLR, 2015.

Y. Song and S. Ermon. Generative modeling by estimating gradients of the data distribution. In H. M. Wallach, H. Larochelle, A. Beygelzimer, F. d'Alché-Buc, E. B. Fox, and R. Garnett, editors, *Advances in Neural Information Processing Systems 32: Annual Conference on Neural Information Processing Systems 2019, NeurIPS 2019, December 8-14, 2019, Vancouver, BC, Canada*, pages 11895–11907, 2019. URL `https://proceedings.neurips.cc/paper/2019/hash/3001ef257407d5a371a96dcd947c7d93-Abstract.html`.

Y. Song and S. Ermon. Improved techniques for training score-based generative models. *Advances in neural information processing systems*, 33:12438–12448, 2020.

Y. Song, S. Garg, J. Shi, and S. Ermon. Sliced score matching: A scalable approach to density and score estimation. In *Uncertainty in Artificial Intelligence*, pages 574–584. PMLR, 2020.

Y. Song, C. Durkan, I. Murray, and S. Ermon. Maximum likelihood training of score-based diffusion models. *Advances in Neural Information Processing Systems*, 34:1415–1428, 2021a.

Y. Song, J. Sohl-Dickstein, D. P. Kingma, A. Kumar, S. Ermon, and B. Poole. Score-based generative modeling through stochastic differential equations. In *9th International Conference on Learning Representations, ICLR 2021, Virtual Event, Austria, May 3-7, 2021*. OpenReview.net, 2021b. URL `https://openreview.net/forum?id=PxTIG12RRHS`.

A. Vahdat, K. Kreis, and J. Kautz. Score-based generative modeling in latent space. *Advances in Neural Information Processing Systems*, 34, 2021.

P. Vincent. A connection between score matching and denoising autoencoders. *Neural computation*, 23(7):1661–1674, 2011.

L. Zhou, Y. Du, and J. Wu. 3d shape generation and completion through point-voxel diffusion. In *2021 IEEE/CVF International Conference on Computer Vision, ICCV 2021, Montreal, QC, Canada, October 10-17, 2021*, pages 5806–5815. IEEE, 2021. doi: 10.1109/ICCV48922.2021.00577. URL `https://doi.org/10.1109/ICCV48922.2021.00577`.

Checklist

1. For all authors...
   (a) Do the main claims made in the abstract and introduction accurately reflect the paper's contributions and scope? [Yes]
   (b) Did you describe the limitations of your work? [Yes] The assumptions are followed by a discussion of their strength.
   (c) Did you discuss any potential negative societal impacts of your work? [Yes] See Section 7.
   (d) Have you read the ethics review guidelines and ensured that your paper conforms to them? [Yes]
2. If you are including theoretical results...
   (a) Did you state the full set of assumptions of all theoretical results? [Yes]

(b) Did you include complete proofs of all theoretical results? [Yes]

3. If you ran experiments...
   (a) Did you include the code, data, and instructions needed to reproduce the main experimental results (either in the supplemental material or as a URL)? [Yes]
   (b) Did you specify all the training details (e.g., data splits, hyperparameters, how they were chosen)? [Yes] See Appendix B.
   (c) Did you report error bars (e.g., with respect to the random seed after running experiments multiple times)? [No] There are no error to report, we just have small illustrative numerical experiments.
   (d) Did you include the total amount of compute and the type of resources used (e.g., type of GPUs, internal cluster, or cloud provider)? [Yes] See Appendix B.
4. If you are using existing assets (e.g., code, data, models) or curating/releasing new assets...
   (a) If your work uses existing assets, did you cite the creators? [N/A] We did not use any existing assets.
   (b) Did you mention the license of the assets? [N/A]
   (c) Did you include any new assets either in the supplemental material or as a URL? [N/A]
   (d) Did you discuss whether and how consent was obtained from people whose data you're using/curating? [N/A]
   (e) Did you discuss whether the data you are using/curating contains personally identifiable information or offensive content? [N/A]
5. If you used crowdsourcing or conducted research with human subjects...
   (a) Did you include the full text of instructions given to participants and screenshots, if applicable? [N/A] We did not use crowdsourcing or conduct research with human subjects.
   (b) Did you describe any potential participant risks, with links to Institutional Review Board (IRB) approvals, if applicable? [N/A]
   (c) Did you include the estimated hourly wage paid to participants and the total amount spent on participant compensation? [N/A]

A Stochastic prerequisites

In this section we give a formal introduction to some of the concepts used in this work. For a more rigorous treatment, see for example [Klenke, 2013] or [Karatzas and Shreve, 2012].

A.1 Equivalence of measures / Girsanov Theorem

First we define absolute continuity of measures. Let μ and ν be two measures on $(\Omega, \mathcal{F})$, where $\mathcal{F}$ is a σ-algebra.

Definition 1. *We say that μ is absolutely continuous with respect to ν if $\mu(A) = 0$ for any $A \in \mathcal{F}$ such that $\nu(A) = 0$. We also denote this by $\mu \ll \nu$.*

Two measures μ and ν are equivalent if $\mu \ll \nu$ and $\nu \ll \mu$. Loosely speaking, we can say that $\mu \ll \nu$ if the support of μ is contained in the support of ν and they are equivalent if they share the same support.

The Radon-Nikodym theorem tells us that if $\mu \ll \nu$, then under mild conditions there exists a density $\frac{\mathrm{d}\mu}{\mathrm{d}\nu} : \Omega \to \mathbb{R}$ such that $\mu(A) = \int_A \frac{\mathrm{d}\mu}{\mathrm{d}\nu}(\omega)\mathrm{d}\nu(\omega)$. Therefore, we can obtain μ through a reweighting of ν. One specific instance of this is the Girsanov Theorem. Assume we are given the solutions to two SDEs in $\mathbb{R}^d$,

$$\mathrm{d}Y_t = b(t, Y_t)\mathrm{d}t + \sigma(t, Y_t)\mathrm{d}W_t \tag{13}$$

and

$$\mathrm{d}\tilde{Y}_t = b(t, \tilde{Y}_t)\mathrm{d}t + \sigma(t, \tilde{Y}_t)e(t, \tilde{Y}_t)\mathrm{d}t + \sigma(t, \tilde{Y}_t)\mathrm{d}B_t. \tag{14}$$

Both of these induce a measure on the space of continuous functions $\Omega = C([0, T], \mathbb{R}^d)$. We denote them by $\mathbb{P}$ and $\tilde{\mathbb{P}}$ respectively. Then the Girsanov Theorem equips us with conditions under which the measures $\mathbb{P}$ and $\tilde{\mathbb{P}}$ are equivalent. Furthermore, in case of equivalence we get a formula for the density of $\tilde{\mathbb{P}}$ with respect to $\mathbb{P}$. The relative density is given as

$$Z_T = \exp\left(\int_0^T e(s, Y_s)\mathrm{d}W_s - \frac{1}{2}\int_0^T \|e(s, Y_s)\|^2 \mathrm{d}s\right).$$

For a full statement of the Girsanov Theorem and under which conditions it holds, see [Karatzas and Shreve, 2012, Section 3.5].

A.2 Uniform integrability

Since we are treating the case where the drift explodes as $t \to T$ we end up with densities

$$Z_t = \exp\left(\int_0^t e(s, Y_s)\mathrm{d}W_s - \frac{1}{2}\int_0^t \|e(s, Y_s)\|^2 \mathrm{d}s\right). \tag{15}$$

on $C([0, t], \mathbb{R}^d)$, but not with a density on $C([0, T], \mathbb{R}^d)$. Uniform integrability is exactly the condition one needs to extend these local densities.

Definition 2. *A family $\{X_\alpha\}$ of random variables is called uniformly integrable if*

$$\sup_\alpha \mathbb{E}\left[|X_\alpha| \, 1_{\{|X_\alpha| > s\}}\right] \to 0$$

as $s \to \infty$.

In the proof of Theorem 2 we implicitly use the following two results which we here state as a lemma. The filtration $\mathcal{F}_t$ is defined as in the proof of Theorem 2.

Lemma 4. *Assume the Z_t in* (15) *form a uniformly integrable martingale on $[0, T)$. Then,*

- *the limit $\lim_{t \to T} Z_t$ exists in L^1. We denote this limit by Z.*
- *Furthermore, $\tilde{\mathbb{P}}$ is absolutely continuous with respect to $\mathbb{P}$ on $\mathcal{F} = \sigma(\cup_{t<T}\mathcal{F}_t)$ with density Z.*

Proof. Both of these results are standard. The first one can for example be found in [Karatzas and Shreve, 2012, Section 1.3.B]. For the second one we compute that for any $A \in \mathcal{F}_s$,

$$\mathbb{E}_{\mathbb{P}}[1_A Z] = \mathbb{E}_{\mathbb{P}}[1_A \lim_{t\to T} Z_t] = \lim_{t\to T} \mathbb{E}_{\mathbb{P}}[1_A Z_t] = \mathbb{E}_{\mathbb{P}}[1_A Z_s] = \mathbb{E}_{\tilde{\mathbb{P}}}[1_A],$$

where we used L^1 convergence in the second equality and the martingale property of Z_s in the third equality. Therefore Z is a density of $\tilde{\mathbb{P}}$ with respect to $\mathbb{P}$ on each $\mathcal{F}_s$ for $s < T$. Therefore Z is also a density of $\tilde{\mathbb{P}}$ with respect to $\mathbb{P}$ on $\mathcal{F}$ which concludes the proof. □

B Numerics

All numerical experiments can be run on a consumer grade computer within a few minutes.

B.1 Figure 1

We first discuss the top left figure of Figure 1. We set $p_0 = \mu_{\text{data}}$ to a mixture of two Gaussian $\mathcal{N}(-2, \frac{1}{100})$ and $\mathcal{N}(2, \frac{1}{100})$ with weights $w_1 = \frac{1}{3}$ and $w_2 = \frac{2}{3}$ respectively. Then, we draw $N = 5\,000\,000$ samples from μ_{data}, denoted by Y_0^n, $n = 1, \dots, N$. An Euler-Maruyama discretization of the Brownian motion propagates these samples from time $t = 0$ to $t = 1$ by

$$X_{i+1}^n = X_i^n + \sqrt{dt} Z_i^n,$$

where $Z_n^i \sim \mathcal{N}(0,1)$ are i.i.d. random variables, independent of X_m^j for $m \le n$ and $j = 1, \dots, N$. The time index i runs from 0 to $I = 2000$ and dt is set to $dt = \frac{1}{I}$. The initial samples $\{X_0^n\}_{n=1}^N$ are used to create the left line plot of p_0 and the final samples $\{X_I^n\}_{n=1}^N$ are used to create the right line plot of p_1 using kernel density estimation. The $\{X_i^n\}_{n=1}^N$ are approximate samples from $p_{i/I}$. Therefore, we create histograms using $\{X_i^n\}_{n=1}^N$ to approximate $p_{i/I}$. The height of the histogram bars corresponds to the square root of the colour intensity in the heat map. The horizontal axis in the heat map stands for the time t, whereas the vertical axis stands for the position x. At location (t, x) we plot an estimate of $\sqrt{p_t(x)}$. We apply the square root since it improves the contrast in areas where $p_t(x)$ is close to 0 and makes it more visible where $p_t(x) > 0$ to the observer.

For the bottom left figure we show the same plots, just for the reverse SDE (8) instead of the forward SDE. Since the initial distribution is a Gaussian mixture we can exactly calculate p_t using

$$p_t(x) = w_1 \mathcal{N}(x; m_1, s_1^2 + t) + w_2 \mathcal{N}(x; m_2, s_2^2 + t), \tag{16}$$

where we use $\mathcal{N}(x; m, v)$ for the probability density function of a normal distribution with mean m and variance v, evaluated at x. With the above expression of p_t one could compute an analytical representation of $\nabla \log p_t$. We use automatic differentiation instead. The reverse SDE (8) is simulated with a disturbance $e(x,t) = 1$ and initial condition $q_0 = \mu_{\text{prior}} = \mathcal{N}(0,1)$. The Euler-Maruyama method is run with the same step size $dt = \frac{1}{I}$. More precisely, the one step transition kernel of the discretized reverse SDE is

$$Y_{i+1}^n = Y_i^n + dt\, (\nabla \log p_{1-\frac{i}{I}}(Y_i^n) + 1) + \sqrt{dt}\, \tilde{Z}_i^n, \tag{17}$$

where $\tilde{Z}_n^i \sim \mathcal{N}(0,1)$ are i.i.d. random variables, independent of Y_m^j for $m \le n$ and $j = 1, \dots, N$. The plots are created in the same way as for the upper left plot, except that we reverse the time axis to plot p_t and q_{1-t} directly underneath each other.

On the right side we plot the same kernel density estimates already plotted on the left side as μ_{sample} and μ_{data} into the same plot for comparison.

B.2 Figure 2b and 2a

Figure 2b is created by setting μ_{data} to be the uniform distribution on $M = 9$ equally spaced samples $\{x_i\}_{i=1}^M$ on the unit sphere $\mathcal{S}^1$. This can also be viewed as a Gaussian mixture with 9 components where each component having mean x_i and variance 0. Therefore, we can again explicitly calculate p_t for $t > 0$ as in (16),

$$p_t(y) = \frac{1}{M} \sum_{i=1}^M \mathcal{N}(y; x_i, t).$$

	$m_t(z_0)$	Σ_t
Brownian Motion	z_0	tI_d
OU-Process	$\exp(-t)z_0$	$(1-\exp(-2t))I_d$

Table 1: The mean and covariance of the Gaussian transition kernels of the Brownian Motion and the Ornstein-Uhlenbeck process SDEs.

The score $\nabla \log p_t(y)$ is evaluated using automatic differentiation. The reverse SDE 8 is simulated with $q_0 = \mathcal{N}((x = -1.5, y = 0), I_2)$ and $e((x, y), t) = (x = 0, y = -1)$. For the numerical simulation, we again use the Euler-Maruyama scheme. We use a step width of $dt = \frac{0.9}{1000} \approx \frac{1}{1000}$ for $t = [0, 0.9]$, $dt = \frac{0.09}{1000} \approx \frac{1}{10\,000}$ for $t \in [0.9, 0.99]$ and of $dt = \frac{1}{100\,000}$ for $t \in [0.99, 1]$. For a simulation of $N = 50\,000$ paths of the reverse SDE, we start by drawing $Y_0^n = A_n + Z_n$, where A_n are i.i.d. uniformly distributed on $\{x_i\}_{i=1}^M$ and $Z_n \sim \mathcal{N}(0, 1)$ i.i.d.. The $\{A_n\}$ and $\{Z_n\}$ are also independent from each other. We then propagate the Y_0^n similarly to (17), except that we use a different values for dt depending on t. This leads to approximate samples Y_t^i from q_t. At the displayed times t we plot the function

$$h_t(x) = \sum_{i=1}^{N} k(x, Y_t^i),$$

where k is an unnormalized Gaussian kernel with a very small bandwidth parameter,

$$k(x, y) = \exp(-1000\|x - y\|^2).$$

Normalizing h_t gives us a density estimate of q_t. We plot these estimates as heat maps for different values of t.

For Figure 2a we follow the same steps as for Figure 2b, except that μ_{data} is set to the uniform distribution over $M = 256$ evenly spaced samples from the unit sphere $\mathcal{S}^1$.

B.3 Figure 3

For Figure 3 we used the DDPM++ model from the Github repository for the paper from Song et al. [2021b]. Then we evaluated the true score using (6), where the sum runs through the $N = 50000$ training examples of CIFAR-10, Krizhevsky et al. [2009]. A similar experiment using the true marginals $\hat{\mu}_{\text{data}}$ has also been conducted in Peluchetti [2021].

C Studying the forward Densities

C.1 Transition kernels

The transition kernels $p(z_0, \cdot)$ for the SDEs from Section 2 are of the from

$$q_0(z_0, \cdot) = \mathcal{N}(m_t(z_0), \Sigma_t),$$

where m_t and Σ_t are given in Table 1 for the Brownian Motion and the Ornstein-Uhlenbeck process. The form of the transition kernels for the CLD are more involved. They can be found in Dockhorn et al. [2021, Appendix B.1].

Lemma 5. *The marginal densities $p_t(x)$ of the SDEs treated in Section 2 depend smoothly on x and t.*

Proof. One can combine the form of m_t and Σ_t and the explicit representation of p_t in (11) to see this. More generally, for the Brownian motion and the OU-Process this is a result of the Hörmander theorem. For the CLD it is a result of hypocoercivity. □

C.2 Form of the drift

We now prove that we can represent the drift as in (12).

Lemma 6. *Assume that p_t has the form* (11)*, i.e.*

$$p_t(z) = \int_{\mathbb{R}^d} \mathcal{N}(z; m_t(z_0), \Sigma_t)\mu_{data}(z_0)\mathrm{d}z_0.$$

Then (12) *holds true, i.e.*

$$\nabla \log p_t = \frac{\nabla p_t(z)}{p_z(z)} = \Sigma_t^{-1}(z - \mathbb{E}[m_t(Z_0)|Z_t = z]).$$

Proof.

$$\begin{aligned}
&\nabla p_t(z) \\
&= \frac{1}{\sqrt{\det(2\pi\Sigma_t)}} \int_{\mathbb{R}^d} \nabla \exp\left(-\frac{1}{2}(z - m_t(z_0))\Sigma_t^{-1}(z - m_t(z_0))\right)\mu_{\text{data}}(z_0)\mathrm{d}z_0 \\
&= \frac{1}{\sqrt{\det(2\pi\Sigma_t)}} \int_{\mathbb{R}^d} \Sigma_t^{-1}(z - m_t(z_0)) \exp\left(-\frac{1}{2}(z - m_t(z_0))\Sigma_t^{-1}(z - m_t(z_0))\right)\mu_{\text{data}}(z_0)\mathrm{d}z_0 \\
&= \Sigma_t^{-1} z p_t(z) \\
&\quad - \frac{1}{\sqrt{\det(2\pi\Sigma_t)}} \int_{\mathbb{R}^d} \Sigma_t^{-1} m_t(z_0) \exp\left(-\frac{1}{2}(z - m_t(z_0))\Sigma_t^{-1}(z - m_t(z_0))\right)\mu_{\text{data}}(z_0)\mathrm{d}z_0.
\end{aligned}$$

If we now divide everything by p_t it cancels in the first summand. In the second summand we get the formula for the conditional expectation (see, for example [Klenke, 2013, Section 8.2]). □

D Reverse SDEs: The general case

One can also treat more general forward SDEs than we did in Section 1. This leads to a more complicated form of the reverse SDE. Our Theorems do not use the specific form of the forward SDEs and therefore also hold in the general case. We denote the forward SDE by

$$\begin{aligned}
\mathrm{d}X_t &= \beta(t, X_t)\mathrm{d}t + \sigma(t, X_t)\mathrm{d}W_t, \\
X_0 &\sim \mu_{\text{data}},
\end{aligned} \tag{18}$$

where μ_{data} is supported on $\mathcal{M} \subset \mathbb{R}^d$ and W_t is a $\mathbb{R}^r$ valued Brownian motion. The drift b maps from $\mathbb{R} \times \mathbb{R}^d$ to $\mathbb{R}^d$. The dispersion coefficient σ maps from $\mathbb{R} \times \mathbb{R}^d$ to the $d \times r$-matrices. The time-reversed process $Y_t := X_{T-t}$ is then a solution to

$$\begin{aligned}
\mathrm{dY}_t &= b(t, Y_t)\mathrm{d}t + \sigma(T - t, Y_t)\mathrm{d}B_t, \\
Y_0 &\sim q_0,
\end{aligned} \tag{19}$$

with

$$b_i(t, y) = -\beta(T - t, y) + \frac{\sum_j \nabla_j(a_{\text{ij}}(T - t, y)p_{T-t}(y))}{p_{T-t}(y)}, \quad a(t, y) = \sigma(t, y)\sigma(t, y)^T,$$

and $q_0 = p_T$, see Haussmann and Pardoux [1986]. This simplifies to the case discussed in Section 1 if $r = d$, σ is is a multiple of the identity matrix and β is independent of the time t. In Assumption 1 we treat the case where the SDEs are of the form written-out in Section 1. The items $(i) - (iii)$ need to be replaced by their more general counterpart as found in Haussmann and Pardoux [1986, Section 2]. In the last item (iv), $\nabla \log p_t$ needs to be replaced by $\frac{\sum_j \nabla_j(a_{\text{ij}}(T-t,y)p_{T-t}(y))}{p_{T-t}(y)}$.

E Proofs

E.1 Proofs of the theorems

We now give proofs of our main results and briefly summarize the key steps in an intuitive way. In our study we would like to include the case when μ_{data} is degenerate and supported on a low-dimensional

substructure $\mathcal{M}$. As we have seen in Section **??**, this can lead to an exploding drift in the reverse SDE as $t \to T$. Nevertheless, in order to understand the properties of μ_{data}, it is crucial to study the properties of solutions to the reverse SDE at time $t = T$. This is where the main mathematical difficulties come from. The proofs are mostly independent of the specific form of the forward SDE and hold for more general forward/backward SDEs than those stated in Section 1, see Appendix D.

E.1.1 Theorem 1

We now proceed with proving Theorem 1.

Proof. Let P be the measure on $\Omega = C([0,T],\mathbb{R}^n)$ induced by the forward SDE (1) started in $p_0 = \mu_{\text{data}}$. P has marginals p_t. Denote by X_t the canonical projections $X_t(\omega) = \omega(t)$ for $\omega \in \Omega$. We define Q through

$$\frac{\mathrm{d}Q}{\mathrm{d}P}(\omega) = \frac{\mathrm{d}\mu_{\text{prior}}}{\mathrm{d}\pi_T}(\omega(T)).$$

By the data processing inequality we obtain (see [Liese and Vajda, 2006, Theorem 14]),

$$KL(q_T|\mu_{\text{data}}) \leq KL(Q|P) = KL(\mu_{\text{prior}}|\pi_T). \tag{20}$$

It remains to prove that by running Q backwards we obtain a solution to (2) started in μ_{prior}. We denote the generator of the reverse SDE (2) by $\mathcal{L}$. Denote by Q^R and P^R the time reversals of Q and P. Our assumption are such that P^R is a Markov process solving the martingale problem for $\mathcal{L}$ (see [Haussmann and Pardoux, 1986, Theorem 2.1]). A short calculation shows that Q^R is still Markov (see, for example [Léonard, 2011, Proposition 4.2]). Furthermore for $f \in C_c^\infty(\mathbb{R}^n)$,

$$\begin{aligned}
&\mathbb{E}_{Q^R}\left[f(X_t) - f(X_s) - \int_s^t \mathcal{L}f(X_r)\mathrm{d}r|X_s\right] \\
&= \frac{\mathbb{E}_{P^R}\left[\left(f(X_t) - f(X_s) - \int_s^t \mathcal{L}f(X_r)\mathrm{d}r\right)\frac{\mathrm{d}\mu_{\text{prior}}}{\mathrm{d}p_T}(X_0)|X_s\right]}{\mathbb{E}_{P^R}\left[\frac{\mathrm{d}\mu_{\text{prior}}}{\mathrm{d}p_T}(X_0)|X_s\right]} \\
&= \frac{\mathbb{E}_{P^R}\left[\left(f(X_t) - f(X_s) - \int_s^t \mathcal{L}f(X_r)\mathrm{d}r\right)|X_s\right]\mathbb{E}_{P^R}\left[\frac{\mathrm{d}\mu_{\text{prior}}}{\mathrm{d}p_T}(X_0)|X_s\right]}{\mathbb{E}_{P^R}\left[\frac{\mathrm{d}\mu_{\text{prior}}}{\mathrm{d}p_T}(X_0)|X_s\right]} \\
&= \mathbb{E}_{P^R}\left[\left(f(X_t) - f(X_s) - \int_s^t \mathcal{L}f(X_r)\mathrm{d}r\right)|X_s\right] = 0.
\end{aligned}$$

In the second equality we used the Markov property of P^R. In the last one we used that P^R solves the martingale problem for $\mathcal{L}$. Therefore also Q^R solves the martingale problem for $\mathcal{L}$. Denote by Y_t a solution to (2) on $[0,T)$. Since solutions to (2) are unique in law on $[0,S]$ for $S < T$ (see [Karatzas and Shreve, 2012, Section 5.2]) and the solutions are continuous, the law of Y is equal to Q^R on $[0,T)$. But the paths of Q^R are continuous on $[0,T]$. Therefore, Y can be extended to $[0,T]$, i.e. the limit $Y_T := \lim_{t\to T} Y_t$ exists almost surely and its distribution is equal to the T-time marginal distribution of Q^R, which is the 0-time marginal of Q. We denote the marginals of Q and P by Q_t and P_t. Since Q is absolutely continuous with respect to P, $Q_0 = \mu_{\text{sample}}$ is absolutely continuous with respect to $P_0 = \mu_{\text{data}}$. Analogously, if μ_{prior} and p_T are equivalent, then so are P and Q and therefore P_0 and Q_0. This proves (i).

(ii) is a consequence of the data processing inequality for f-divergences ([Liese and Vajda, 2006, Theorem 14]), analogous to (20). □

The main idea of this proof is that we look at the forward SDE for X_t first. It induces a distribution $\mathbb{P}$ over all continuous paths in $\Omega = C([0,T],\mathbb{R}^d)$. If we reverse the time direction of this distribution on Ω, we get a solution to the reverse SDE, started in p_T. This reverse solution is well behaved as $t \to T$, since $Y_T = X_0$. The solution for a different initial condition $\mu_{\text{prior}} \neq p_T$ is obtained by reweighting $\mathbb{P}$. This does not change the qualitative behaviour of Y_T, which still exists and is well defined. We then use a uniqueness result to see that any solution of (19) inherits these properties.

E.1.2 Theorem 2

Proof. Denote the space $C([0,T),\mathbb{R}^d)$ by Ω. We also define the natural filtration $\mathcal{F}_t = \sigma(x(s)|s \leq t)$. We denote the distribution of Y on Ω by $\mathbb{P}$. We define $\tilde{\mathbb{P}}$ by reweighting $\mathbb{P}$ with Z_t on $\mathcal{F}_t$. By Girsanov theorem (see [Karatzas and Shreve, 2012, Section 3.5]) we know that the canonical process under $\tilde{\mathbb{P}}$ is a solution to (8) on $[0,T)$. Since Z_t is uniformly integrable, its limit $Z := \lim_{t\to T} Z_t$ exists in L^1. Furthermore $\tilde{\mathbb{P}}$ is absolutely continuous with respect to $\mathbb{P}$ on $\mathcal{F} = \sigma(\cup_{t<T}\mathcal{F}_t) = \sigma(x(t)|t<T)$ with density Z. We define $x(T) := \lim_{t\to T} x(t)$. Then the event

$$\mathcal{A} = \{x(T) := \lim_{t\to T} x(t) \text{ exists and } x(T) \in \mathcal{M}\}$$

has probability 1 under $\mathbb{P}$ (see Theorem 1) and therefore also under $\tilde{\mathbb{P}}$. Furthermore, $x(T)$ is measurable with respect to $\mathcal{F}$. Therefore the distributions of $x(T)$ under $\mathbb{P}$ and $\tilde{\mathbb{P}}$ are equivalent. The canonical process under $\tilde{\mathbb{P}}$ is therefore a solution of (8), with the property that its time T-marginal is well defined and equivalent to the time T-marginal of (2). We can use uniqueness in law on $[0,S)$ for any $S<T$ and extend it to $[0,T]$ as in the proof of Theorem 1. This shows that every solution to (8) has the desired properties.

Finally we show that if e is bounded, it fulfils Assumptions 2. We define by $H_t = \int_0^t \|e(s,\hat{Y}_s)\|\mathrm{d}s$. Then there is a Brownian motion W_t such that we can write Z_t as

$$Z_t = \exp\left(W_{H_t} - \frac{1}{2}H_t\right).$$

Since e is bounded by M, H_t is bounded by TM. In particular, one can view $Z_t = \mathbb{E}[Z_{TM}|\mathcal{F}_{H_t}]$. Therefore Z_t is uniformly integrable since it can be viewed as a family of conditional expectations. □

Here we essentially applied the Girsanov Theorem on $[0,T)$. Using the uniform integrability of the Girsanov weights Z_t, we are able to extend it to $[0,T]$. Therefore, we can infer that the distribution of Y and $\hat{Y}$ are actually equivalent on the whole path space $C([0,T],\mathbb{R}^d)$. In particular, their time T-marginals will be equivalent too, which is the claim of the theorem.

E.2 Proof of the Lemmas

We start by proving Lemma 1.

Proof. The forward drifts are $\beta(x) = 0$, $\beta(x) = -\frac{\alpha}{2}x$ and $\beta(x,v) = (v, -x-2v)$ for the Brownian Motion, the OU-Process and the Critically Damped Langevin Dynamics respectively. In particular, these are all linear maps and therefore fulfil conditions (i) and (ii) of Assumption 1.

We show in Appendix C.1 that $\log p_t$ is C^∞ in t and x for $t>0$. Therefore we can integrate p_t and its derivative over compact sets, implying that condition (iii) holds. Furthermore, the Hessian w.r.t. (x,t) is continuous and obtains its maximum and minimum on the compact set $[S,T]\times B_N$, where B_N is the ball of diameter N around the origin. Therefore the gradient $\nabla \log p_t$ is Lipschitz on $[S,T]\times B_N$, which proves (iv). □

We now prove Lemma 2.

Proof. We have that $X_0 \sim \mu_{\text{data}}$. Denote the mean and covariance of μ_{data} by a and C respectively. We define

$$n_t = \mathcal{N}(m_t, V_t)$$

for some functions m_t and V_t. If V_t would not have full rank, n_t would be a degenerate distribution. Since $p_t > 0$ almost everywhere for $t>0$, the KL divergence from p_t to n_t would be infinite. We can therefore restrict V_t to be an invertible matrix. We denote the entropy of p by H, $H(p) = -\int \log(p)p\mathrm{d}x$.

We can write X_t as $X_t = X_0 + \sqrt{t}Z$ where $Z \sim \mathcal{N}(0, I_d)$. Now for the KL-divergence at time t it holds that

$$\begin{aligned} KL(p_t|n_t) &= -H(p_t) - \int \log(n_t(x))p_t(x)\mathrm{d}x \\ &= -H(p_t) + \frac{d}{2}\log(2\pi) + \frac{1}{2}\log\left(\det(V_t)\right) + \frac{1}{2}\int (x-m_t)^T V_t^{-1}(x-m_t)\, p_t(x)\mathrm{d}x. \end{aligned}$$

We compute

$$\begin{aligned} &\int (x-m_t)^T V_t^{-1}(x-m_t)\, p_t(x)\mathrm{d}x \\ &= \mathbb{E}[(X_t-m_t)^T V_t^{-1}(X_t-m_t)] = \mathbb{E}[(X_0+\sqrt{t}Z-m_t)^T V_t^{-1}(X_0+\sqrt{t}Z-m_t)] \\ &= \mathbb{E}[(X_0-a)^T V_t^{-1}(X_0-a)] + (a-m_t)^T V_t^{-1}(a-m_t) + t\mathbb{E}[Z^T V_t^{-1} Z] \\ &= \mathrm{tr}(CV_t^{-1}) + t\,\mathrm{tr}(I_d V_t^{-1}) + (a-m_t)^T V_t^{-1}(a-m_t). \end{aligned}$$

We added and subtracted a in the second equality. In the last equality we used that $\mathbb{E}[X^T A X] = \mathrm{tr}(\mathrm{Cov}(X)A)$ if X is a centred random variable. Substituting this into our prior calculation, we arrive at

$$\begin{aligned} &KL(p_t|n_t) \\ =\ & -H(p_t) + \frac{1}{2}\log\left(\det(2\pi V_t)\right) + \frac{1}{2}\left(\mathrm{tr}((C+tI_d)V_t^{-1}) + (a-m_t)^T V_t^{-1}(a-m_t)\right). \end{aligned}$$

The mean function m_t only appears in the last term. Therefore, we decrease the KL-divergence by setting $m_t = a$. We now optimize for the covariance matrix V_t. The $H(p_t)$ term is independent of V_t. Consequently, to optimize the $KL(p_t|n_t)$ with respect to V_t, it is enough to optimize

$$\begin{aligned} L(V_t^{-1}) &= \log\left(\det(V_t)\right) + \mathrm{tr}((C+tI_d)V_t^{-1}) \\ &= -\log\left(\det(V_t^{-1})\right) + \mathrm{tr}((C+tI_d)V_t^{-1}), \end{aligned}$$

where we used that $\det(A^{-1}) = \det(A)^{-1}$ to rewrite the loss in terms of V_t^{-1}. Since $-\log(\det(\cdot))$ is convex on the positive semidefinite matrices and the other summands are linear, L is convex in V_t^{-1}. We take the gradient of L with respect to the Frobenius inner product and obtain

$$\nabla_{V_t^{-1}} L(V_t^{-1}) = -V_t + C + tI_d.$$

Setting the gradient to 0 has the unique solution

$$V_t = C + tI_d,$$

which is a local and global minimum due to the convexity of L.

If we restrict V_t to be of the form $V_t = v_t I_d$, the loss becomes

$$L(v_t^{-1}) = -d\log(v_t^{-1}) + v_t^{-1}\mathrm{tr}(C) + v_t^{-1}td.$$

By setting the derivative of this to zero, we arrive at

$$v_t = \mathrm{tr}(C)/d + t.$$

□

We now proceed to prove Lemma 3. For that we first need the following proposition.

Proposition 1. *Let p_t be the time t-marginal of a Brownian motion started in μ_{data}. Assume that the support of μ_{data} is contained in a ball of radius M. Let $m_t = \mathbb{E}[\mu_{data}]$ and $C_t = Cov[\mu_{data}] + tI_d$ be the optimal mean and covariance operator from Lemma 2. Denote $n_t = \mathcal{N}(m_t, V_t)$. Then $KL(p_t|n_t) \to 0$ as $t \to \infty$.*

Proof. For $t > 0$, the KL-divergence is given by

$$\begin{aligned} KL(p_t|n_t) &= -H(p_t) + \frac{1}{2}\log\left(\det(2\pi V_t)\right) + \frac{1}{2}\mathrm{tr}((C+tI_d)V_t^{-1}) \\ &= -H(p_t) + \frac{1}{2}\log\left(\det(2\pi V_t)\right) + \frac{d}{2} \\ &= -H(p_t) + \frac{d}{2}\log(2\pi) + \frac{1}{2}\log\left(\prod_{i=1}^{d}(c_i+d)\right) + \frac{d}{2}. \end{aligned} \tag{21}$$

We used that

$$\det(C + tI_d) = \prod_{i=1}^{d}(c_i + t), \tag{22}$$

where c_i are the eigenvalues of $\mathrm{Cov}[\mu_{\text{data}}]$.

Now,

$$-H(p_t) = \mathbb{E}_{X_t}[\log p_t(X_t)] = \mathbb{E}_{X_t}\left[\log\left(\mathbb{E}_{X_0}\left[(2\pi t)^{-d/2}\exp\left(-\frac{1}{2t}\|X_t - X_0\|^2\right)\right]\right)\right].$$

We bound

$$\exp\left(-\frac{1}{2t}\|X_t - X_0\|^2\right) \leq \exp\left(-\frac{1}{2t}(\|X_t\|^2 - 2\|X_t\|M)\right).$$

We write X_t as $X_t = X_0 + \sqrt{t}Z$ where $Z \sim \mathcal{N}(0, I_d)$. Then,

$$\begin{aligned}
&\log\left(\mathbb{E}_{X_0}\left[(2\pi t)^{-d/2}\exp\left(-\frac{1}{2t}\|X_t - X_0\|^2\right)\right]\right) \\
&\leq \log((2\pi t)^{-d/2}) - \frac{1}{2t}(\|X_t\|^2 - 2\|X_t\|M) \\
&\leq -\frac{d}{2}\log(2\pi) - \frac{1}{2}\log(t^d) - \frac{1}{2t}\|X_t\|^2 + \frac{1}{t}(\|M\| + \sqrt{t}\|Z\|)M.
\end{aligned} \tag{23}$$

We use that

$$\mathbb{E}[\|X_t\|^2] = \mathbb{E}[\|X_0\|^2] + t\mathbb{E}[\|Z\|^2] = \mathbb{E}[\|X_0\|^2] + t\mathbb{E}[\|Z\|^2] = m_0^2 + v_0 + td,$$

where $v_0 = \mathbb{E}[\|X_0 - \mathbb{E}[\mu_{\text{data}}]\|^2] = \mathrm{tr}(C_0)$. Since Z is centred and independent of X_t, the cross-term $\mathbb{E}[\langle X_t, Z\rangle] = 0$ vanishes. We now take the expectation over the right hand side of (23) to obtain

$$\mathbb{E}[-\frac{1}{2t}(\|X_t\|^2 - \|X_t\|M)] \leq \frac{1}{2t}\left(-td - m_0 - v_0 + 2\sqrt{t}\mathbb{E}[\|Z\|]M + 2M^2\right).$$

Putting it all together we have that

$$KL(p_t|n_t) \leq \frac{1}{2}\log\left(\frac{\prod_{i=1}^{d}(c_i + t)}{t^d}\right) + \frac{1}{2t}\left(-m_0 - v_0 + 2\sqrt{t}\mathbb{E}[\|Z\|]M + 2M^2\right) \to 0,$$

as $t \to \infty$. □

We are now ready to prove Lemma 3.

Proof. We again use (21). We now take the derivative of the KL-divergence using De Bruijn's identity for multivariate random variables (see [Rioul, 2010], [Costa and Cover, 1984]):

$$\frac{\mathrm{d}}{\mathrm{d}t}H(p_t) = \frac{1}{2}\mathbb{E}_{p_t}[\|\nabla \log p_t(X)\|^2] = \frac{1}{2t^2}\mathbb{E}[\|X_t - \mathbb{E}[X_0|X_t]\|^2], \tag{24}$$

where we applied Lemma 6. Since $\mathbb{E}[X_0|X_t]$ is the L^2-orthogonal projection of X_0 to the $\sigma(X_t)$-measurable random variables and X_t is $\sigma(X_t)$-measurable, we have that

$$\frac{1}{2t^2}\mathbb{E}[\|X_t - \mathbb{E}[X_0|X_t]\|^2] = \frac{1}{2t^2}\left(\mathbb{E}[\|X_t - X_0\|^2] - \mathbb{E}[\|X_0 - \mathbb{E}[X_0|X_t]\|^2]\right) = \frac{d}{2t} - \frac{A_t}{2t^2}.$$

For $A_t = \mathbb{E}[\|X_0 - \mathbb{E}[X_0|X_t]\|^2]$ it holds that

$$0 \leq A_t \leq \mathbb{E}[\|X_0\|^2] = \mathrm{tr}(\mathrm{Cov}(\mu_{\text{data}})),$$

since the conditional expectation is a contraction in L^2. We use (22) again to arrive at

$$\frac{\mathrm{d}}{\mathrm{d}t}KL(p_t|n_t) = -\frac{1}{2}\left(\frac{d}{t} - \frac{A_t}{t^2}\right) + \frac{1}{2}\sum_{i=1}^{d}\frac{1}{t + c_i} \geq -\frac{1}{2}\frac{d}{t} + \frac{1}{2}\sum_{i=1}^{d}\frac{1}{t + c_i} =: h'(t), \tag{25}$$

where c_i are the eigenvalues of $\text{Cov}[\mu_{\text{data}}] + tI_d$. Integrating the right hand side we obtain

$$h(t) = \frac{1}{2} \log \left(\frac{\prod_{i=1}^d (c_i + t)}{t^d} \right)$$

as a possible antiderivative. Define $g(t) = h(t) - KL(p_t|n_t)$. Let us now assume that the support of μ_{data} is contained in a ball of radius M. Then, by Proposition 1, $\lim_{t\to\infty} KL(p_t|n_t) = \lim_{t\to\infty} h(t) = 0$ and therefore $\lim g(t) \to 0$. Equation (25) implies that $g'(t) \leq 0$ for all $t > 0$. Assume that there is a s and an $\epsilon > 0$ such that $g(s) \leq -\epsilon < 0$. Since $g'(t) \leq 0$ for all $t > 0$ we can then conclude that $g(t) \leq -\epsilon < 0$ for all $t \geq s$. In particular, $g(t) \not\to 0$ as $t \to \infty$, which is a contradiction. Therefore the statement of the Lemma holds for μ_{data}.

Now let μ_{data} be any measure. Let X be a random variable that is distributed according to μ_{data} and Z be a standard normal random variable, $Z \sim \mathcal{N}(0, I_d)$. Then $X + \sqrt{t}Z$ has distribution p_t. We define $X^M := X 1_{\{\|X\| \leq M\}}$ and $X_t^M = X^M + \sqrt{t}Z$. Denote the distribution of X_t^M by p_t^M. The distribution of X^M is supported on a ball of radius M. Furthermore, $X^M + \sqrt{t}Z \to X + \sqrt{t}Z$ almost surely and therefore $p_t^M \to p_t$ weakly for any t. By lower semi-continuity of the KL-divergence,

$$KL(p_t|n_t) \leq \liminf_{M\to\infty} KL(p_t^M|n_t) \leq \liminf_{M\to\infty} \frac{1}{2} \log \left(\frac{\prod_{i=1}^d (c_i^M + t)}{t^d} \right), \tag{26}$$

where c_i^M are the eigenvalues of $\text{Cov}[\mu_{\text{data}}^M] + tI_d$. Since $|X^M| \leq |X|$ and X has first and second moments one can apply dominated convergence to see that the covariance matrices converge, $\text{Cov}(\mu_{\text{data}}^M) \to \text{Cov}(\mu_{\text{data}})$. Especially

$$\lim_{M\to\infty} \prod_{i=1}^d (c_i^M + t) = \lim_{M\to\infty} \det(\text{Cov}(\mu_{\text{data}}^M)) \to \det(\text{Cov}(\mu_{\text{data}})) = \prod_{i=1}^d (c_i + t).$$

Combining this with (26) concludes the proof. □